The Journal of Chemical Physics

# $CH_4$, an *ab initio* story of an archetypal species

Cite as: J. Chem. Phys. **156**, 214303 (2022); https://doi.org/10.1063/5.0088788
Submitted: 20 February 2022 • Accepted: 15 May 2022 • Published Online: 01 June 2022

Apostolos Kalemos



The Journal of Chemical Physics ARTICLE scitation.org/journal/jcp

# $CH_4$, an *ab initio* story of an archetypal species

Cite as: J. Chem. Phys. 156, 214303 (2022); doi: 10.1063/5.0088788
Submitted: 20 February 2022 • Accepted: 15 May 2022 •
Published Online: 1 June 2022



Apostolos Kalemos[a)]

AFFILIATIONS

Department of Chemistry, Laboratory of Physical Chemistry, National and Kapodistrian University of Athens, Athens 157 71, Greece

**Note:** This paper is part of the JCP Special Topic on Nature of the Chemical Bond.
[a)]**Author to whom correspondence should be addressed:** kalemos@chem.uoa.gr

## ABSTRACT

The methane molecule is an archetypal species in the whole of chemistry for its ability to form four bonds that result in a myriad of compounds of chemical and biological importance. The hybrid orbitals involved in the bonding have been scrutinized for too many decades but only lately under the *ab initio* microscope. In this study, we detail the formation routes $CH_n + (4 - n)\,H \rightarrow CH_4$ ($n = 0$, 1, and 2) both diabatically and adiabatically with the help of established computational techniques. The evolution of the Mulliken populations, of the non-adiabatic matrix coupling elements, and of the Kotani spin functions along the dissociation paths and finally the shape of the diabatic curves unambiguously point to a parental C atom of an excited $2s^1 2p^3$ electronic configuration.



## I. INTRODUCTION

A stable molecular system is a bound collection of electrons and nuclei described by the stationary solutions of the Schrödinger equation tagged by quantum numbers that specify the representations of the various components of the full symmetry group. Although this is correct, there is nothing that reminds us of its "classical" definition as understood by an ordinary chemist, i.e., a group of atoms glued together by chemical bonds depicted as straight bars and positioned into various places in space while the formation of the molecular edifice follows the Lewis theory of valence. The chemical bond, central and one of the most sacred concepts in chemistry, is certainly not an observable,[1,2] but nevertheless, it is the crown jewel of the field. Along with the concept of the molecular structure, they have shaped the way we experience chemistry and they act as a path along which quantum actuality is projected and understood as a chemical reality.

Within the context of quantum chemistry, the concept of the chemical bond is realized through the molecular orbitals obtained primarily from mean field theories like Hartree-Fock (HF) or multi configuration HF, and they are in most of the cases symmetry orbitals. Although such a quality is aesthetically appealing, it does not conform to a chemist's view of a localized chemical bond. To address this issue, a number of localization procedures have been invented; see, e.g., Ref. 3 and references therein. Another way toward the (visual) consideration of the "chemical bond" is through the spin coupled generalized valence bond (SCGVB) wavefunction[4–7] that retains the simplicity of a Hartree product and at the same time respects both the spin symmetry and the Pauli principle. Moreover, it addresses the so-called non-dynamical problem as it inherently contains essential double excitations[8] out of the RHF wave function when written in its natural orbital representation.[9] The resulting mostly localized SCGVB orbitals form the basis for an "objective" interpretation of chemical phenomena (see, e.g., Refs. 10–12) since they sort out in alignment with the well-established chemical concepts without any prejudices. Their form and continuous evolution along any reaction coordinate have led to interesting and useful interpretations of the chemical data but do not detail the origin of the quantum states of the fragments involved.[13]

Toward this end, we combine the virtues of the existing computational methods for the construction of both the adiabatic and diabatic potential energy curves coupled with the evolution of the non-adiabatic coupling matrix elements (NACME) and the Kotani spin functions along selected reaction paths in order to understand the bonding situation of the ground $CH_4$ species.

## II. THE $CH_4$ STORY

One of the earliest $CH_4$ studies, similar in character with the present work, appears to be the SCGVB contribution by Hay *et al.*[14] who studied the complete $CH_n$ series by single point calculations.

The $^3$P carbon atomic state features two oppositely directed *sp* lobes (*sx* and $\overline{sx}$ in their terminology)[15] and two pure *p* orbitals along the *y* and *z* axes. The SCGVB *sp* lobes contain a 13% of *p* symmetry ($sp^{0.15}$ character) as found with a DZ basis set. The CH ($X^2\Pi$) state forms naturally by coupling an H atom to the pure $2p_z$ electron while the SCGVB lone pair orbitals bend back from the CH bond at an angle of 128°. The hybrid orbital of its bond has a 81.5% of *p* contribution while that of the lone pair a 25.7% (or $sp^{0.35}$). The $a^4\Sigma^-$ state arises by decoupling its ($^3$P) *sx*, $\overline{sx}$ electron pair, and forming a CH bond while it features a $sp^{0.53}$ bonding hybrid and a $sp^{0.72}$ sigma lobe. The $^1A_1$ $CH_2$ molecular state is formed when a second H atom binds to the spin defining electron of CH ($X^2\Pi$). Its bonding orbital has now a 78.5% *p* contribution while its lone pair lobe is of $sp^{0.76}$ character. The formation of a new (second) CH bond with one of the (decoupled) *sp* lobes of CH ($X^2\Pi$) gives rise to the $CH_2$ ($^3B_1$) state whose hybrid orbitals have a 51.5% (bonding) and 72.4% (lobe) *p* contribution. By attaching two H atoms to the $^3B_1$ $CH_2$ state, the ground $CH_4$ species is formed with a bonding hybrid of 70.3% of *p* symmetry or $sp^{2.3}$ character.

Along a similar vein, Penotti *et al.*[16] computed SCGVB/[4*s*2*p*1*d*/2*s*1*p*] orbitals. Four of the eight valence orbitals are localized on the four hydrogen atoms and resemble the atomic 1*s* functions while the rest are localized on carbon and are visually similar to Pauling's $sp^3$ hybrid orbitals but as analyzed by Cook[17] they are only of $sp^{0.9}$ character in sharp contrast to the numerical findings ($sp^{2.3}$) of Hay *et al.*[14]

Based on calculations in both the coordinate and the momentum space Wang[18] concluded in 2004 that the electronic structure of methane inherited that of the free single carbon atom in its $^3$P state, and there are no quantitative evidences of hybrization of its molecular orbitals. Her analysis though did not consider at all the electronic details of the $^5$S carbon state.

Shaik *et al.*[19] in a 2017 study performed valence bond self consistent field (VBSCF)/6-31 G(d) calculations where purely localized orbitals were free to adjust variationally devoid of constraints or conceptual preconceptions. They hence obtained four tetrahedral orbitals of $sp^{1.76}$ character, a numerical result that balances the increased strength of the CH bonds associated with carbon's $^5$S ($2s^12p^3$) state and the high promotion energy to reach it. Based on their analysis this $^5$S state participates by an amount of 59% exactly as concluded by Voge[20] and cited in Pauling's book.[21]

In a 2019 SCGVB study on $XH_n$ ($n$ = 1–4, X = C, Si, and Ge), Xu *et al.*[22] reported on the formation sequence X → XH → $XH_2$ → $XH_3$ → $XH_4$. The spirit and the strategy of their work are identical to the one by Hay *et al.*[14] and consequently they reached the same conceptual conclusions although their numerical data differ. The SCGVB $CH_4$ orbitals are of $sp^{0.58}$ character in sharp contrast with the historically accepted $sp^3$ hybrids but in close agreement with the results found by Penotti *et al.*[16,17] The evolution of the SCGVB $sp^n$ character along the sequence C → CH → $CH_2$ → $CH_3$ → $CH_4$ reads: $sp^{0.15}$ [C ($^3$P), lone pair] → $sp^{1.56}$ [CH ($X^2\Pi$), bond orbital], $sp^{0.28}$ [CH ($X^2\Pi$), lone pair], $sp^{0.30}$ [CH ($a^4\Sigma^-$), bond orbital], $sp^{0.28}$ [CH ($a^4\Sigma^-$), $\sigma$ lobe] → $sp^{0.42}$ [$CH_2$ ($\tilde{X}^3B_1$), bond orbital], $sp^{0.85}$ [$CH_2$ ($\tilde{X}^3B_1$), $\sigma$ lobe], $sp^{1.63}$ [$CH_2$ ($\tilde{a}^1A_1$), bond orbital], $sp^{0.56}$ [$CH_2$ ($\tilde{a}^1A_1$), lone pair] → $sp^{0.51}$ [$CH_3$ ($^2A_1$), bond orbital] → $sp^{0.59}$ [$CH_4$ ($^1A_1$), bond orbital]. Although all of the molecular states considered presumably result from the C ground $^3$P state[14,22] the composition of the hybrid orbitals involved ranges from 0.15 to 1.56 to 0.59. So, we should not rely only on such a parameter in order to conclude on the atomic pedigree of the final species.

The above results prompted Xu and Dunning[23] to pursue the $CH_4$ problem further through a more focused and detailed study. They reported on $CH_4$'s $sp^n$ character along the computational sequence RHF ($sp^{2.72}$) → SCGVB(PP/SO) ($sp^{2.97}$) → SCGVB(PP) ($sp^{1.58}$) → SCGVB ($sp^{0.57}$). Based on these numerical results and the Skaik *et al.*[19] way of analysis, they suggested that the SCGVB "picture" of C ($^3$P) accounts for its tetravalency without the need to invoke the highly excited $^5$S state.

All of the above findings suggest that the mixing of different angular momentum functions that gives rise to the SCGVB hybrids arise from the physics of the problem and not from any presupposed rules or prescriptions that are primarily due to point group symmetry. So, the orbital composition has nothing to do with the well known Pauling rules while the latter has nothing to do with the notion of electron promotion.[24]

Intrigued by these results and the conceptual points stated or implied in the past, we wanted to further elaborate the question of the carbon nature inside $CH_4$ from an atom[13] based perspective rather than from an orbital point of view.

## III. COMPUTATIONAL DETAILS

We have studied the formation of $CH_4$, both diabatically and adiabatically, along several formation paths written symbolically as $CH_n$ + (4 − $n$) H → $CH_4$, where $n$ = 0, 1, and 2 through valence state average complete active space SCF (SACASSCF), complete active space valence bond (CASVB), and MRCI computations coupled with the (aug)–cc–pVQZ basis set. The active spaces of the SACASSCF calculations are as follows:

SACASSCF($5e^-$/5orb, 2 states) for the C + H → CH ($^4\Sigma^-$) interaction (Fig. 1), SACASSCF($5e^-$/5orb, 4 states) for the C + H → CH ($^2\Delta$) interaction (Fig. 2), SACASSCF($6e^-$/6orb, 2 states) for the CH + H → $CH_2$ ($^3A''$) interaction (Fig. 3), SACASSCF ($6e^-$/16orb, 20 states) for the CH + H → $CH_2$ ($^1A''$) interaction (Fig. 4), SACASSCF($8e^-$/12orb, 10 states) for the $CH_2$ + 2H → $CH_4$ interaction (Fig. 5), SACASSCF($8e^-$/8orb, 3 states) for the $CH_2$ + 2H → $CH_4$ interaction (Fig. 6), SACASSCF($8e^-$/12orb, 20 states) for the CH + 3H → $CH_4$ interaction (Fig. 7), and SACASSCF($8e^-$/12orb, 22 states) for the C + 4H → $CH_4$ interaction (Fig. 8).

The electronic character of the $CH_n$ fragments has also been detailed by the evolution of the spin functions and NACMEs computed by finite differences with a step of 0.01 Å along the considered reaction paths. The MOLPRO computational package[25] has been used in this work.

## IV. RESULTS AND DISCUSSION

In order to reveal the character of the C atom inside the final $CH_4$ species, we have studied the $CH_n$ + (4 − $n$) H → $CH_4$ ($n$ = 0, 1, and 2) reaction routes both diabatically and adiabatically. Consequently, our analysis will be built upon the valence atomic and molecular states of the fragments involved, namely C,[26] CH,[27] and $CH_2$.[28] In what follows, we detail the relevant states of the constituent fragments.

At the ROHF level, the C ($^3$P) atom has $2s^{2.0}2p^{2.0}$ Mulliken atomic populations, while at the CASSCF (2*s*, 2*p*) level, these

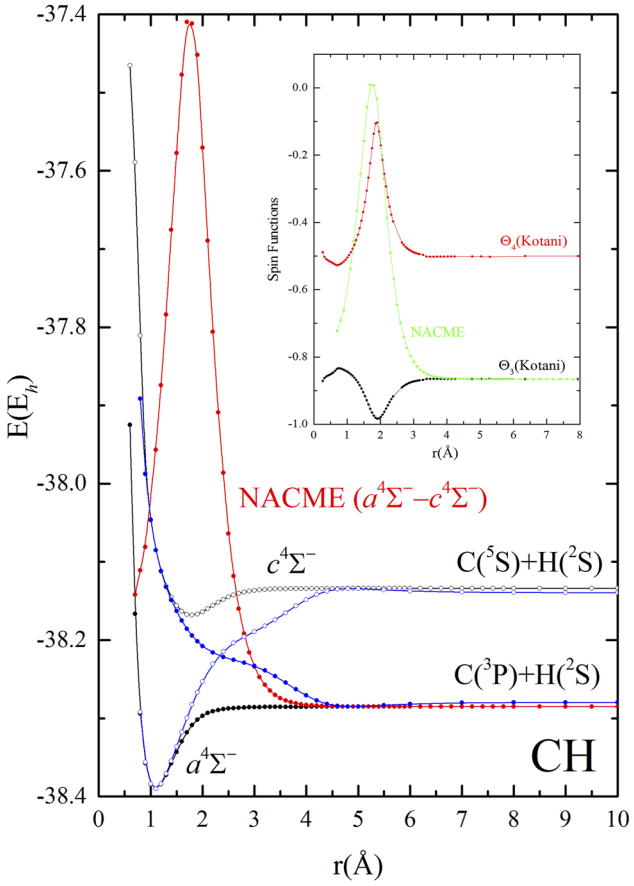


**FIG. 1.** MRCI/aug–cc–pVQZ adiabatic and diabatic potential energy curves of the $a^4\Sigma^-$ and $c^4\Sigma^-$ CH states and their associated (properly translated) NACMEs (Å$^{-1}$). The Kotani $\Theta_3$ and $\Theta_4$ spin functions contrasted with the (translated and scaled) NACMEs are displayed in the inset. At infinity, the order of the SCGVB orbitals is $2s_-1s2s_+2p_x2p_y$.

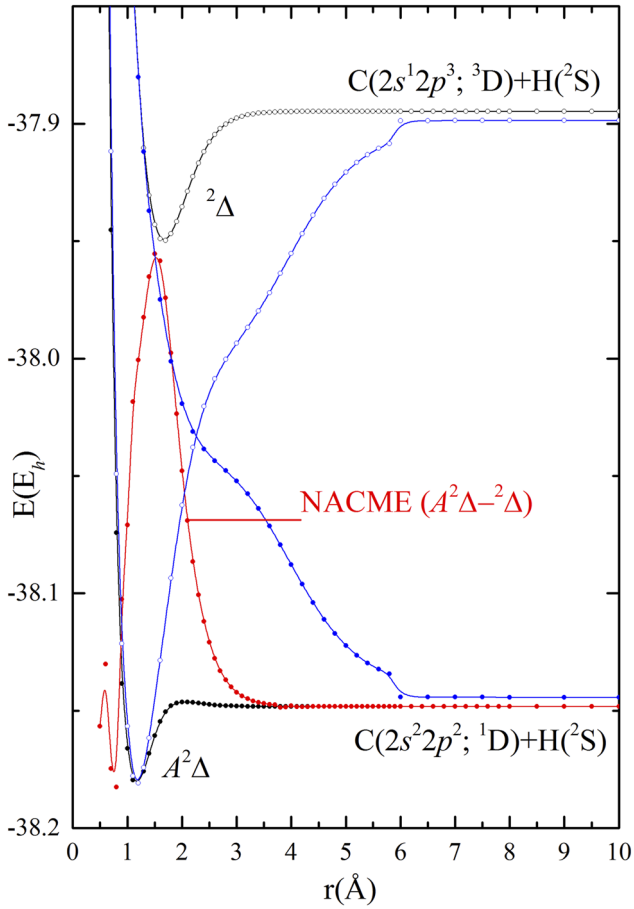


**FIG. 2.** SACASSCF(5e$^-$/5orb, 4 states)/aug–cc–pVQZ adiabatic and diabatic potential energy curves of the $^2\Delta$ CH states dissociating to C ($2s^22p^2$; $^1$D) and C ($2s^12p^3$; $^3$D) along with their corresponding (translated and scaled) NACMEs (Å$^{-1}$).

are $2s^{1.96}2p^{2.04}$ reflecting the (SCGVB) relaxation[15] offered by the enlarged active space and the formation of atomic hybrid orbitals.

In CH ($X^2\Pi$), these atomic distributions remain largely unchanged, i.e., $2s^{1.97}2p_x^{0.98}2p_y^{0.05}2p_z^{1.23}$ with the 0.23 ($2p_z$) electronic excess reflecting the charge migration from the H 1 *s* state. Thus, the C atom is *in situ* in a quasi undisturbed atomic $^3$P state as previously reported.[14,27]

In CH ($a^4\Sigma^-$), we have $2s^{1.48(0.48=0.30+0.18)}2p_x^{1.0}2p_y^{1.0}2p_z^{0.82(=1.0-0.18)}$ with the C atom acquiring an electronic charge of 0.3 electrons from H and distributed over the C 2*s* function. Both CASSCF and SCGVB wave functions give identical energies so the above Mulliken populations reflect the character of the SCGVB orbitals. But what is its electronic pedigree? An analysis based on the evolution of the NACMEs shows that its equilibrium structure mirrors the C ($^5$S) atomic state (see Fig. 1) due to the interaction of the $a\ ^4\Sigma^-$ [← C ($^3$P) + H ($^2$S)] and $c\ ^4\Sigma^-$ [← C ($^5$S) + H ($^2$S)] potential energy curves. The completely parallel evolution of both the NACMEs and the Kotani spin functions ($\Theta_3$ and $\Theta_4$) [centered at ~1.7 Å (= 3.2 bohr)] clearly suggest that the spin decoupling–recoupling mechanism is due to the carbon $^5$S atomic state; see also the discussion in Ref. 27. Finally, the shape of the (crossing) diabatic potential energy curves (see Fig. 1) leaves no doubt on the *in situ* excited state ($^5$S) of the C atom inside the CH $a^4\Sigma^-$ state.

The CH ($A^2\Delta$) state originates adiabatically[27] from C ($^1$D) + H ($^2$S) while its molecular $^2$A$_2$ symmetry component correlates with the atomic $^1$A$_2$ ($^1$D) $[=\left|2s^2(2p_x^12p_y^1)_{\text{singlet}}\right|_{\text{RHF}}]$ projection. The CASSCF (2*s*, 2*p*) Mulliken distributions and the SCGVB hybrid $sp^{0.15}$ orbitals of C ($^1$A$_2$) are $2s^{1.95}2p_z^{0.04}2p_x^{1.0}2p_y^{1.0}$ and $2s_\pm$ = 0.93 (2*s*) ± 0.36 ($2p_z$), respectively. Interestingly enough, the SCGVB hybrid orbitals of the carbon $^3$P ($^3$A$_2$) = $\left|(2s_+^12s_-^1)_{\text{singlet}}2p_x^12p_y^1\right|$ and $^1$D ($^1$A$_2$) = $\left|(2s_+^12s_-^12p_x^12p_y^1)_{\text{singlet}}\right|$ states are practically the same, so from their form alone one cannot distinguish their atomic origin. The CASSCF populations of CH ($A^2\Delta$) are $2s^{1.65}2p_z^{0.75}2p_x^{0.97}2p_y^{0.97}/_C1s^{0.57}(p)^{0.06}$

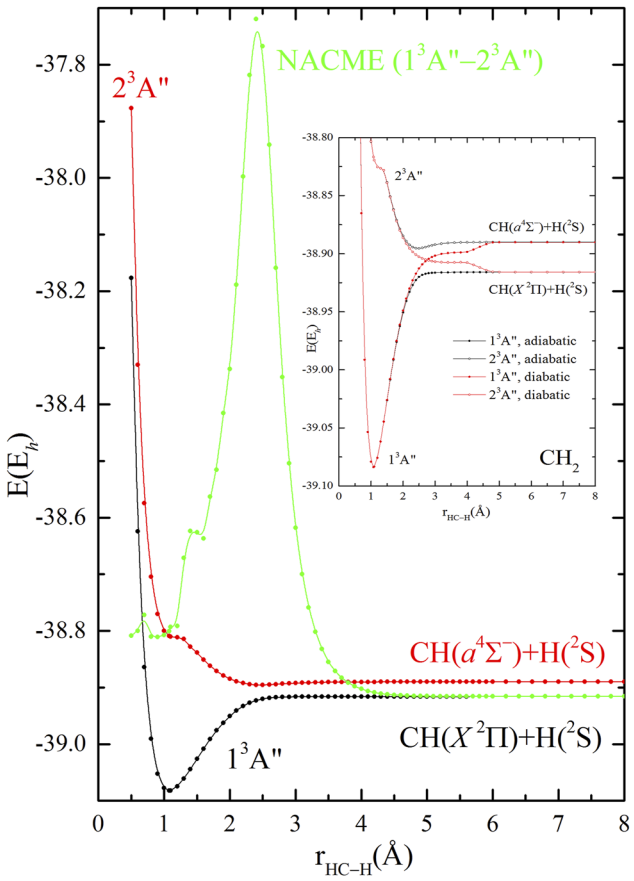


**FIG. 3.** MRCI/aug–cc–pVQZ potential energy profiles of the ground $\tilde{X}\,^3B_1$ and the first excited $^3A''$ $CH_2$ states along the HC + H dissociation path with the CH distance and the HCH angle at the equilibrium values of $\tilde{X}\,^3B_1$. Their corresponding (translated and scaled) NACMEs (Å$^{-1}$) are also displayed. The diabatic energy profiles are shown in the inset.

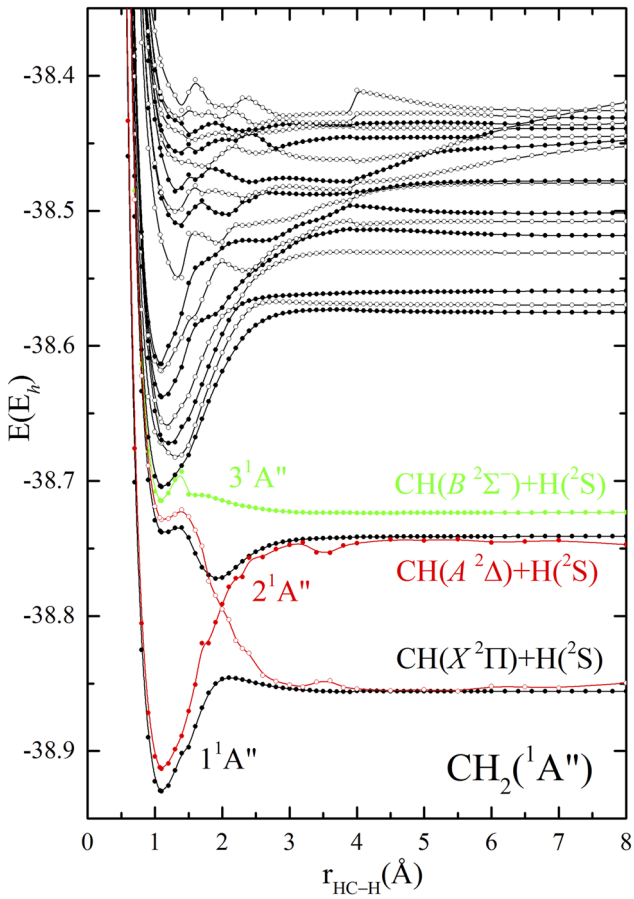


**FIG. 4.** Adiabatic and diabatic energy profiles of the $\tilde{b}\,^1B_1$ and excited $^1A''$ $CH_2$ states along the HC + H dissociation path at the SACASSCF(6e$^-$/16orb, 20 states)/aug–cc–pVQZ level of theory. The CH distance and the HCH angle remain fixed at the equilibrium values of the $\tilde{b}\,^1B_1$ state.

with q (C) = −0.36 clearly reminiscent of the C [$^3$D ($2s^1 2p^3$)] state (see also the discussion in Ref. 27). The CH ($A^2\Delta$) bond formation is characterized by a large charge transfer of ~0.4$e^-$ and an internal migration (from $2p_z$) of ~0.25$e^-$ both directed to the $2s_-$ hybrid orbital. So, its parental atomic state is C ($^3$D) although adiabatically it correlates with C ($^1$D) as clearly seen by the shape of the (crossing) diabatic curves (Fig. 2). This is also in complete agreement with the evolution of the NACMEs [centered at ~1.5 Å (= 2.8 bohr)] that shows exactly the transmittance of the excited $^3$D carbon state in CH ($A^2\Delta$); see Fig. 2.

The ground $CH_2$ ($\tilde{X}\,^3B_1$) state acquires at linearity a $^3\Sigma_g^-$ symmetry with an inversion barrier of 5.7 kcal/mol while the $^3\Sigma_g^-$ configuration correlates directly to CH ($a^4\Sigma^-$) + H ($^2$S) with a binding energy of 116.5 kcal/mol.[28] The CH ($a^4\Sigma^-$) radical offers two ways of attack, a linear (HCH, $^3\Sigma_g^-$) and a perpendicular [$CH_2$, $^3B_1(\theta = 90°)$], the mixing of these two limiting cases gives rise to the actual geometry of the ground state [$\theta(\tilde{X}) \cong 134° \cong (180° + 90°)/2$]. The Mulliken atomic distributions of $CH_2$ ($\tilde{X}\,^3B_1$) read $2s^{1.55}2p_x^{0.96}2p_y^{1.20}2p_z^{0.89}(d)^{0.04}$ ($yz$ is the molecular plane) with an overall charge of −0.66 (=−0.33 × 2) distributed primarily over the $2s$ (0.55) and less on the $2p_y 2p_z$ (0.09) functions, and this situation is clearly similar to the one previously discussed for the CH ($a^4\Sigma^-$) state. It is interesting and illuminating at the same time to consider breaking the $CH_2$ species from its equilibrium configuration. Following the $CH_2 \rightarrow CH + H$ dissociation path, the $\tilde{X}\,^3B_1$ state dissociates adiabatically to CH ($X^2\Pi$) + H ($^2$S) but at the expense of an avoided crossing with the curve originating adiabatically from CH ($a^4\Sigma^-$) + H ($^2$S); see Fig. 3. The change of the electronic character is mirrored in the evolution of the NACMEs with its maximum at ~ 2.4 Å (= 4.5 bohr). So, $CH_2$ ($\tilde{X}\,^3B_1$) correlates diabatically to CH ($a^4\Sigma^-$) as the corresponding diabatic potential energy curves clearly show (see the inset of Fig. 3).

The $\tilde{a}\,^1A_1(\theta = 102°)$ and $\tilde{b}\,^1B_1(\theta = 142°)$ $CH_2$ states[28] become at linearity the degenerate Renner–Teller partners of a $^1\Delta_g$ configuration that dissociates adiabatically to CH ($A^2\Delta$) + H ($^2$S). The rather large inversion barrier of $\tilde{a}\,^1A_1$ (ΔE = 26.4 kcal/mol)[28] favors CH ($X^2\Pi$) as its parental state while the low inversion barrier of

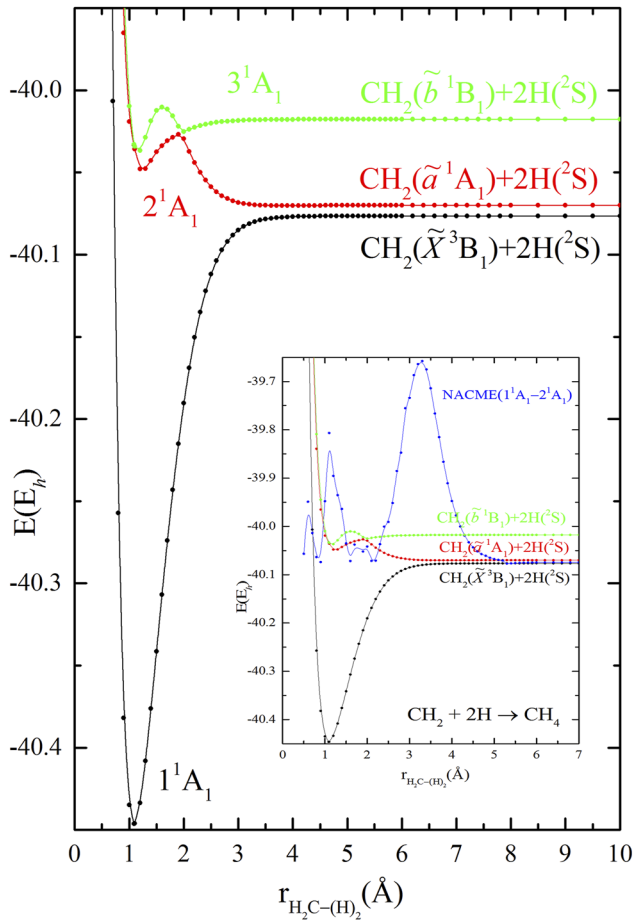


**FIG. 5.** MRCI/cc–pVQZ adiabatic potential energy profiles of the first three $CH_4$ states along the $CH_2$ ($\tilde{X}\,^3B_1$, $\tilde{a}\,^1A_1$, and $\tilde{b}\,^1B_1$) + 2H formation path. The properly translated and scaled NACMEs ($1^1A_1 - 2^1A_1$) ($Å^{-1}$) are displayed in the inset. The CH distances and the HCH angles remain fixed at the equilibrium values of $CH_4$.

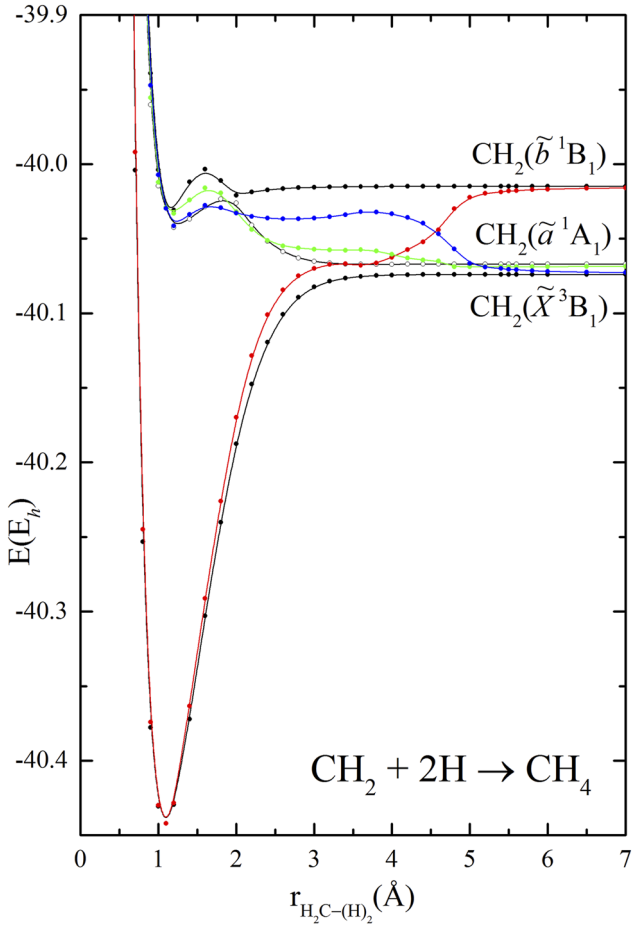


**FIG. 6.** MRCI/cc–pVQZ diabatic potential energy profiles of the first three $CH_4$ states along the $CH_2$ ($\tilde{X}\,^3B_1$, $\tilde{a}\,^1A_1$, and $\tilde{b}\,^1B_1$) + 2H formation path.

$\tilde{b}\,^1B_1$ ($\Delta E$ = 2.7 kcal/mol)[28] suggests CH ($A^2\Delta$) as its ancestral state. This is in line with the atomic populations of the $\tilde{a}\,^1A_1$ state $2s^{1.81}2p_x^{0.09}2p_y^{1.11}2p_z^{1.41}(d)^{0.07}$ with $q$ (C) = −0.50 (=−0.25 × 2), again the $2s^{1.81}$ population mirrors the CH ($X^2\Pi$) state, the electronic excess is being hosted by the $2p_y$ (0.11) and $2p_z$ (0.41) functions. An analysis of the electronic details of the $CH_2$ ($\tilde{a}\,^1A_1$) → CH + H dissociation path shows that it clearly results from CH ($X^2\Pi$).

Concerning the electronic details of $CH_2$ ($\tilde{b}\,^1B_1$) it is found that they are similar to those of its triplet $\tilde{X}\,^3B_1$ analog.[28] Although it correlates adiabatically to CH ($X^2\Pi$) + H ($^2$S) its diabatic character emanates from the CH ($A^2\Delta$) + H ($^2$S) asymptote due to an intense avoided crossing at around 2 Å (see also the diabatic curves in Fig. 4). Its Mulliken atomic distributions $2s^{1.66}2p_z^{0.88}2p_x^{0.94}2p_y^{1.26}(d)^{0.05}/_C1s^{0.54}(p)^{0.06}$ with q(C) = −0.80 (= −0.40 × 2) are in complete agreement with those of the CH ($A^2\Delta$) state (see the above discussion).

Thus, the excited C states are responsible for the formation of both CH and $CH_2$ and this can be written symbolically as C ($^3$P) → CH ($X^2\Pi$) → $CH_2$ ($\tilde{a}\,^1A_1$), C ($^5$S) → CH ($a^4\Sigma^-$) → $CH_2$ ($\tilde{X}\,^3B_1$), and finally C ($^3$D) → CH ($A^2\Delta$) → $CH_2$ ($\tilde{b}\,^1B_1$).

Having detailed the electronic characteristics and atomic origin of both the CH and $CH_2$ molecular fragments, we are now ready to consider the intricacies of the $CH_2$ + 2H → $CH_4$ ($\tilde{X}\,^1A_1$) ← CH + 3H formation routes.

$CH_4$ ($\tilde{X}\,^1A_1$) dissociates adiabatically to $CH_2$ ($\tilde{X}\,^3B_1$) + 2H ($^2$S) (see Fig. 5). This is pretty much expected due to symmetry reasons although the spatial orientation of the triplet coupled electrons in $CH_2$ does not lead to a tetrahedral species as is the case with the $\tilde{a}\,^1A_1$ state that features four C centered SCGVB orbitals[22] with a quasi $T_d$ arrangement. Unexpectedly as it may sound, the $CH_4$ formation is initially mediated through $CH_2$ ($\tilde{a}\,^1A_1$) as a result of an intense avoided crossing peaked at ~3.3 Å (= 6.2 bohr) (see the inset of Fig. 5). The electronically stressful situation of the $CH_2$ ($\tilde{X}\,^3B_1$) + 2H ($^2$S) interaction is reflected in the repulsiveness of the $2^1A_1$ [← $CH_2$ ($\tilde{a}\,^1A_1$) + 2H ($^2$S)] curve for $r < 6.2$ Å that is abruptly terminated at around 2.0 Å (= 3.8 bohr) where a second severe interaction is observed with the potential curve originating from $CH_2$ ($\tilde{b}\,^1B_1$) + 2H ($^2$S); see Fig. 5. This second avoided

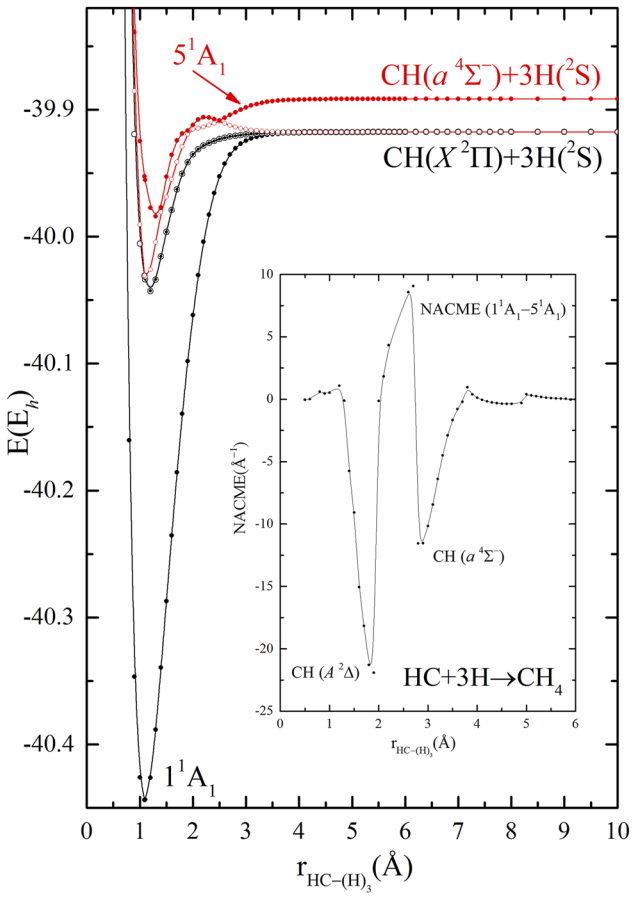


**FIG. 7.** MRCI/cc–pVQZ potential energy profiles of the first five $CH_4$ states along the CH ($X^2\Pi$, $a^4\Sigma^-$) + 3H formation path. The corresponding NACMEs ($1^1A_1 - 5^1A_1$) ($Å^{-1}$) are shown in the inset. The peaks of the NACMEs curve are tagged with the CH character that passes on from $5^1A_1$ to $1^1A_1$. The CH distance and the HCH angles remain fixed at the equilibrium values of $CH_4$.

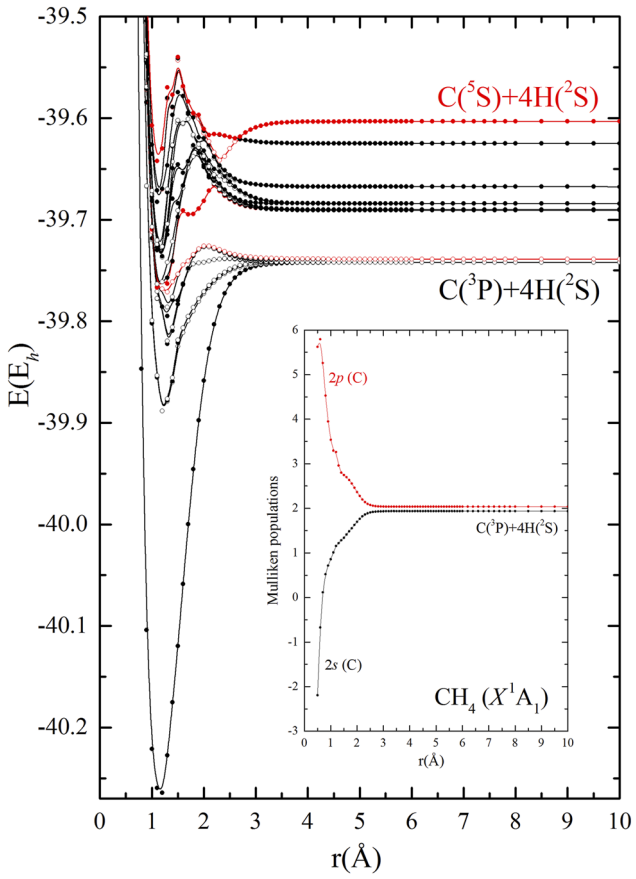


**FIG. 8.** Potential energy profiles of the ground and excited $^1A_1$ $CH_4$ states along the C + 4H dissociation path at the SACASSCF(8e⁻/12orb, 22 states)/cc–pVQZ level of theory. The 2*s* and 2*p* Mulliken populations of the ground curve are displayed in the inset.

crossing gives rise to a shallow minimum but with substantial consequences in its equilibrium character as evidenced by the NACMEs peak at ~1.1 Å (= 2.08 bohr). Consequently, the $CH_2$ ($\tilde{b}^1B_1$) [← CH ($A^2\Delta$) ← C ($^3$D)] character passes on to $CH_4$. The atomic Mulliken populations $2s^{1.28}2p_x^{1.16}2p_y^{1.16}2p_z^{0.16}(d)^{0.11}$ are indicative of this situation. The charge $q$ (C) = −0.88 (=−0.22 × 4) is hosted by the 2*s* (0.28) and 2*p* (0.16 × 3) and *d* (0.11) functions, thus alluding to a $2s^12p^3$ parental atomic state in harmony with the evolution of the NACMEs. In a completely analogous way, the diabatic curves of this 3 × 3 case study (Fig. 6) reveal the *in situ* excited $\tilde{b}^1B_1$ (← $A^2\Delta$ ← $^3$D) state of the $CH_2$ fragment inside ground $CH_4$.

We are now going to observe the formation of $CH_4$ along the CH + 3H path; see Fig. 7. Both chemical wisdom and computational evidence corroborate on the initially important role played by CH ($a^4\Sigma^-$), a state that offers three ready to bind electrons; see the form of the curves in Fig. 7 and the peak (~2.5 Å) of their associated NACMEs (see the inset of Fig. 7). A second crucial peak (~2.0 Å) suggests the participation of the CH ($A^2\Delta$) [← C($^3$D)] character inside the ground $CH_4$ species.

Finally, we shall briefly comment on the C + 4H formation path (see Fig. 8). The interaction of the curve arising from C ($^5$S) + 4H ($^2$S) with the ones below is evident, and this is also reflected on the depopulation of 2*s*, and the synchronous population of the 2*p* orbitals along the reaction coordinate (see the inset of Fig. 8).

## V. CONCLUSIONS

We have studied the $CH_4$ species along the C + 4H, CH + 3H, and $CH_2$ + 2H formation paths by SACASSCF, CASVB, and MRCI methods with the goal to elucidate the nature of the *in situ* fragments, i.e., C, CH, and $CH_2$. All of our computational evidence unambiguously shows the excited nature of CH and $CH_2$ inside $CH_4$ that is ultimately due to the *in situ* excited 2 $s^12p^3$ electronic configuration of C projected as either a $^3$D or a $^5$S atomic state, depending on the symmetry of the fragmentation route.

Since the molecular Hamiltonian is composed of nuclei and electrons and not of atoms or some other fragments, one may say that the bonding in molecular systems is independent of the atomic states, that is, the electrons in the molecule have no memory of what the electron configuration might have been in the bare atom. Certainly, this point of view is not wrong. The idea of a chemical bond has a meaning only within the context of quantum chemistry since a proper quantum mechanical calculation is not compatible with the chemical concepts we have built over the years. However, in the realm of quantum chemistry, i.e., when the rules of quantum mechanics are projected on the "plane" of the Born–Oppenheimer approximation, the "picture" that we get for the electronic structure of $CH_4$ is that of a parental C atom of an excited $2s^1 2p^3$ nature.

## ACKNOWLEDGMENTS

Professor Brian T. Sutcliffe is warmly thanked for reading and commenting on the manuscript.

## AUTHOR DECLARATIONS

### Conflict of Interest

The author has no conflicts to disclose.

## DATA AVAILABILITY

The data that support the findings of this study are available from the corresponding author upon reasonable request.

## REFERENCES

[1] C. A. Coulson, J. Chem. Soc. 2069 (1955).
[2] B. T. Sutcliffe, Phys. Bull. **28**, 360 (1977).
[3] T. Giovannini and H. Koch, J. Chem. Theory Comput. **17**, 139 (2021).
[4] M. Kotani, A. Amemiya, E. Ishiguro, and T. Kimura, *Table of Molecular Integrals* (Maruzen Co., Tokyo, 1955).
[5] J. Gerratt, Annu. Rep. Prog. Chem., Sect. A **65**, 3 (1968).
[6] R. C. Ladner and W. A. Goddard III, J. Chem. Phys. **51**, 1073 (1969).
[7] SCGVB as a special case of the more general projected quasiparticle theory based on the symmetry projected Hartree Fock Bogoliubov equations, see G. E. Scuseria, C. A. Jiménez-Hoyos, T. M. Henderson, K. Samanta, and J. K. Ellis, J. Chem. Phys. **135**, 124108 (2011).
[8] O. Sinanoğlu, Adv. Chem. Phys. **14**, 237 (1969).
[9] A. C. Hurley, J. E. Lennard-Jones, and J. A. Pople, Proc. R. Soc. London, Ser. A **220**, 446 (1953); see also F. W. Bobrowicz and W. A. Goddard III, in *Modern Theoretical Chemistry: Methods of Electronic Structure Theory*, edited by H. F. Schaefer III (Plenum Press, NY, 1977), Vol. 3, Chap. 4.
[10] T. H. Dunning, Jr., L. T. Xu, T. Y. Takeshita, and B. A. Lindquist, J. Phys. Chem. A **120**, 1763 (2016).
[11] T. H. Dunning, Jr. and P. Jeffrey Hay, "Beyond Molecular Orbital Theory: The Impact of Generalized Valence Bond Theory in Molecular Science," in *Computational Materials, Chemistry and Biochemistry: From Bold Initiatives to the Last Mile*, edited by S. Shankar, R. Muller, T. Dunning and G. H. Chen (Springer Cham, 2021), Vol. 284, p. 55.
[12] T. H. Dunning, Jr., L. T. Xu, D. L. Cooper, and P. B. Karadakov, J. Phys. Chem. A **125**, 2021 (2021).
[13] W. Moffitt, Proc. R. Soc. London, Ser. A **210**, 245 (1951).
[14] P. Jeffrey Hay, W. J. Hunt, and W. A. Goddard III, J. Am. Chem. Soc. **94**, 8293 (1972).
[15] Hybrid orbitals as solutions of the H atom in the prolate spheroidal coordinate system, see e.g., C. A. Coulson and P. D. Robinson, Proc. Phys. Soc., London **71**, 815 (1958).
[16] F. Penotti, J. Gerratt, D. L. Cooper, and M. Raimondi, J. Mol. Struct.: THEOCHEM **169**, 421 (1988).
[17] D. B. Cook, J. Mol. Struct.: THEOCHEM **169**, 79 (1988).
[18] F. Wang, J. Mol. Struct.: THEOCHEM **678**, 105 (2004).
[19] S. Shaik, D. Danovich, and P. C. Hiberty, Comput. Theor. Chem. **1116**, 242 (2017).
[20] H. H. Voge, J. Chem. Phys. **4**, 581 (1936); , **16**, 984 (1948).
[21] L. Pauling, *The Nature of the Chemical Bond*, 3rd ed. (Cornell University Press, 1960), pp. 111–120.
[22] L. T. Xu, J. V. K. Thompson, and T. H. Dunning, Jr., J. Phys. Chem. A **123**, 2401 (2019).
[23] L. T. Xu and T. H. Dunning, Jr., J. Phys. Chem. A **124**, 204 (2020).
[24] M. Francl, Nat. Chem. **10**, 688 (2018).
[25] H.-J. Werner, P. J. Knowles, G. Knizia, F. R. Manby, M. Schütz, P. Celani, W. Györffy, D. Kats, T. Korona, R. Lindh, A. Mitrushenkov, G. Rauhut, K. R. Shamasundar, T. B. Adler, R. D. Amos, A. Bernhardsson, A. Berning, D. L. Cooper, M. J. O. Deegan, A. J. Dobbyn, F. Eckert, E. Goll, C. Hampel, A. Hesselmann, G. Hetzer, T. Hrenar, G. Jansen, C. Köppl, Y. Liu, A. W. Lloyd, R. A. Mata, A. J. May, S. J. McNicholas, W. Meyer, M. E. Mura, A. Nicklaß, D. P. O'Neill, P. Palmieri, D. Peng, K. Pflüger, R. Pitzer, M. Reiher, T. Shiozaki, H. Stoll, A. J. Stone, R. Tarroni, T. Thorsteinsson, and M. Wang, MOLPRO, version 2012.1, a package of *ab initio* programs, University College Cardiff Consultants Limited, Cardiff, UK, 2008.
[26] A. Kramida, Yu. Ralchenko, J. Reader, and NIST ASD Team, NIST Atomic Spectra Database (ver. 5.9), National Institute of Standards and Technology, Gaithersburg, MD, 2021, available at https://physics.nist.gov/asd.
[27] A. Kalemos, A. Mavridis, and A. Metropoulos, J. Chem. Phys. **111**, 9536 (1999).
[28] A. Kalemos, T. H. Dunning, Jr., A. Mavridis, and J. F. Harrison, Can. J. Chem. **82**, 684 (2004).